A Pipeline Route Drawing System Equipped With a Towed Unit Using Only Low Cost Internal Sensors

Chihiro Hirose, Shunsuke Ota, Atsushi Kakogawa, *Member, IEEE*, and Shugen Ma, *Fellow, IEEE*

***Abstract*—Conventional systems for drawing pipeline routes from inside of the pipe often use external sensors such as cameras or lasers, but these can be easily affected by the illumination inside of the pipes and the material. Additionally, many of these sensors are high cost and too large to be implemented in small-diameter pipes. Therefore, this study proposes a pipeline route drawing system that uses a towed unit with only low cost internal sensors, which is towed by a self-propelled in-pipe inspection robot. This unit is equipped with only an internal measurement unit (IMU) and an encoder, making it suitable for use in 3- and 4-in pipes without illuminating the inside. The present article describes the method of estimating transition points between straight and curved pipes, the direction of straight pipes after passing through curved pipes, and the position of the curved pipes to be interpolated. Following this, the developed towed unit is used to perform route drawing experiments. The mean absolute error of the route dimension was 1.38% or less under all conditions, and the mean error in estimating the straight pipe direction was approximately 1.35° or less.**

***Index Terms*—Dead reckoning, inspection robots, mechanism design, simultaneous localization and mapping (SLAM).**

I. Introduction

WATER and gas pipes, among others, are widely used worldwide and have become essential for both our daily lives and industrial activities. However, the large-scale aging of these pipes has become a significant concern in recent years. Due to the possibility of toxic hydrogen sulfide and flammable gas flowing through the pipes, urgent pipe inspections are necessary. However, it is costly and time-consuming to manually perform the entire pipeline inspection process. Additionally, it can be challenging to inspect pipelines installed in the ground, at high elevations, or with a small inner diameter. As a result, active researches have been conducted on in-pipe inspection robots [1], [2], [3], [4], [5], [6], [7], [8], [9], [10], [11], [12], [13]. These robots are designed not only to traverse the pipeline but also to accurately identify the 3-D coordinates of corrosion and cracks. Research on drawing pipe routes while running inside of the pipe has gained attention due to its potential benefits.

Previous investigations on the construction of pipeline maps and routes can be broadly divided into three categories. The first is the 3-D reconstruction of pipes through the utilization of point cloud data [1], [2], [3], [4]. However, the pipes targeted in [1] and [2] are large, and no verification has been conducted on small-diameter pipes. Additionally, the light detection and ranging (LiDAR) sensor used in [3] is 62 × 120 × 66 mm and the depth camera used in [4] is 90 × 25 × 25 mm, which are large and not inexpensive. These sensors are physically challenging for pipes with an inner diameter of less than 3 in, and even for 4-in pipes, they may be difficult depending on the curvature radius.

The second category is the drawing of pipeline routes while classifying the type of pipe [5], [6], [7], [8], [9], [10]. Since all pipeline courses can be classified into straight pipes and branch pipes, the pipeline route can be drawn if the rotation direction of the branch pipe is identified. Although camera-based methods have been proposed for this identification [5], [6], [7], these methods have been found to be easily affected by the illumination and dirt inside of the pipes [10]. Therefore, to solve these problems, a method for identifying the rotation direction of the branch pipe using a laser has been proposed [8], [9], [10]. However, if a dedicated image sensor is used to detect the laser light, a separate sensor for the laser is required, which adds extra cost. In addition, the size and mechanism of the laser tends to be generally large. For example, the laser used in [9] is 37 × 48 × 166 mm with a long shaft, making it unsuitable for the curvature of pipes with an inner diameter of less than 4 in. The method proposed in [8] and [10] requires a mechanism to rotate the laser around the pipe axis, which is also unsuitable for small-diameter pipes.

The third category is the drawing of pipeline routes using only internal sensors [11], [12], [13]. Generally, it has been difficult to draw accurate routes using only internal sensors due

Manuscript received 8 February 2024; revised 14 May 2024; accepted 11 June 2024. *(Corresponding author: Atsushi Kakogawa.)*

Chihiro Hirose, Shunsuke Ota, and Atsushi Kakogawa are with the Department of Robotics, Faculty of Science and Engineering, Ritsumeikan University, Shiga 5258577, Japan (e-mail: chihiro_hirose@mail.toyota.co.jp; kakogawa@fc.ritsumei.ac.jp).

Shugen Ma is with The Hong Kong University of Science and Technology (Guangzhou), Guangzhou 511453, China (e-mail: shugenma@hkust-gz.edu.cn).

Color versions of one or more figures in this article are available at https://doi.org/10.1109/TIE.2024.3419240.

Digital Object Identifier 10.1109/TIE.2024.3419240

Fig. 1. Overview of the developed towed sensing system. AIRo-2.6 is a self-propelled in-pipe inspection robot and AIRo-mini-3.0 is a towed sensing unit.

TABLE I
COMPARISON OF THE PREVIOUSLY METHOD [13] AND THIS STUDY

Method	Orientation Estimation	Straight Pipe Direction	Rotation Angle of the Curved Pipe
Previous method [13]	Madgwick filter	$\pm X, \pm Y, \pm Z$	$\frac{\pi}{2}$
This study	Madgwick filter or DMP	Any	Any or $\frac{\pi}{12}$ interval

to the influence of robot vibration and wheel slip. Additionally, measuring multiple joint angles inside of the robot tends to increase the size of the structure [11]. Therefore, Guo et al. [12] demonstrated that accurate drawing is possible using only internal sensors by constructing a multi-internal measurement unit (IMU) system in which multiple IMUs are arranged orthogonally on a W-shaped pipe inspection robot [14]. However, this method requires multiple IMUs, which complicates the internal structure of the robot or increases the total length and computational cost.

As mentioned above, each method possesses certain challenges. Furthermore, the design of robots that travel in pipes must take spatial constraints into account. To address this, we have researched the use of a towed sensing unit (Fig. 1), which is pulled by a self-propelled in-pipe inspection robot, to draw pipeline routes [13]. The unit is equipped with an IMU and an encoder. Measurement errors that arise from using only internal sensors can be resolved by classifying the type of pipe obtained from its standard.

Table I presents a comparison between the previously proposed method [13], and the method of this study. In the previous method, only one type of orientation estimation method, which is called the Madgwick filter [15], was used, but in this study, orientation estimation by digital motion processor (DMP) that uses the built-in processor of the IMU (InvenSense Inc., MPU-6050) is also verified. Regarding the straight pipe direction, only the direction along the Earth frame ($\pm X, \pm Y$, and $\pm Z$ directions) was considered, but in this study, any direction is available. Therefore, the possible rotation angle of the curved pipes is not limited to $\pi/2$. However, since many of the rotation angles of the curved pipe are multiples of $\pi/12$, this study also proposes a correction method using this information.

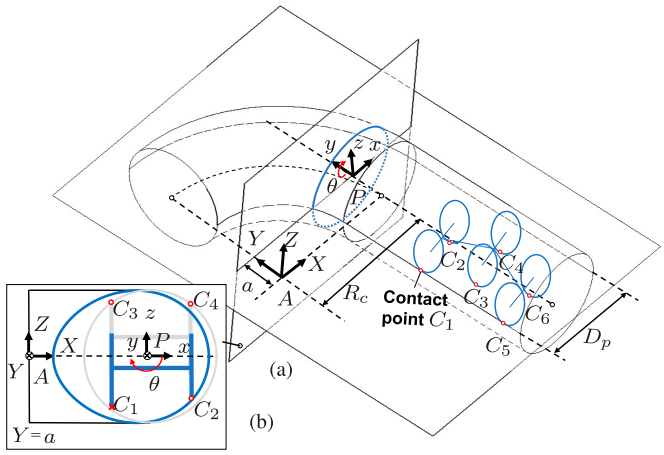

Fig. 2. Geometric model of a V-shaped unit traveling in a curved pipe.

II. DESIGN OF THE TOWED UNIT CAPABLE OF PASSIVELY NAVIGATING CURVED PIPES

A V-shaped linkage unit is a suitable option for small-diameter pipes due to its ability to increase wheel diameter and high step-climbing performance. Therefore, this study utilizes a V-shaped expansion/contraction mechanism for our towed sensing unit. Typically, a V-shaped linkage unit cannot travel curved pipes unless its joint axis and the rotation axis of the curved pipe are aligned [16]. However, there are also V-shaped units that passively rotate their posture from multiple entry angles to travel curved pipes [17]. In this section, the passive rotation principle of the V-shaped unit is clarified, and the conditions for the V-shaped sensing unit to travel curved pipes in all entry postures are derived.

Fig. 2(a) shows the geometric model of a V-shaped unit when entering a curved pipe. In a right-handed coordinate system with the entrance direction of the curved pipe as the X-axis and the exit direction as the Y-axis, the absolute coordinate system A (XYZ) is set at the center of the circle with the curvature radius R_c of the curved pipe. Then, the coordinate system P (xyz) is set by translating the absolute coordinate system A by R_c in the X-axis direction and the displacement a in the Y-axis direction. The contact points between the pipe and the wheels are from C_1 to C_6.

Consider the case in which the unit enters the curved pipe, and the front wheel contacts the wall of the curved pipe on the plane $Y = a$ [Fig. 2(a)]. At this time, both contact points C_1 and C_2 contact the wall of the curved pipe only when the rotation axis of the curved pipe and the joint axis of the unit are aligned, i.e., when the unit can pass through it without the need for posture rotation. When entering in a posture that requires posture rotation, one of the contacts C_1 and C_2 separates [Fig. 2(b)]. Therefore, the moment that passively rotates the unit inside of the curved pipe can be attributed to only one contact point.

First, the cross-sectional shape of the curved pipe cut on the plane $Y = a$ is determined. As shown in Fig. 2, θ is set around the y-axis, the curvature radius of the curved pipe is R_c, and

the inner diameter of the pipe is D_p. Then, the cross-section $C_a(\theta) = (C_{a,X}(\theta), C_{a,Z}(\theta))$ of the curved pipe cut on the plane $Y = a$ can be expressed as follows:

$$C_{a,X}(\theta) = \sqrt{\left(R_c + \frac{D_p}{2}\cos\theta\right)^2 - a^2} \tag{1}$$

$$C_{a,Z}(\theta) = -\frac{D_p}{2}\sin\theta. \tag{2}$$

When the front wheel of the unit enters the curved pipe, it contacts the egg-shaped curved pipe wall, as shown in Fig. 2(b). At this time, the forces acting on the front wheel, i.e., the frictional force and the normal force, are involved in the roll rotation of the unit. Based on this, to cause passive roll rotation when entering a curved pipe, it is necessary to focus on the following two points.

1) Suppress the influence of frictional force that hinders roll rotation.
2) When the unit cannot pass through the curved pipe, apply the normal force to promote roll rotation.

A. Method of Suppressing the Influence of Frictional Force

In the case of a general nonholonomic wheel, a large frictional force occurs in the direction perpendicular to the rotation direction of the wheel. Since the direction of this frictional force coincides with the direction in which the unit rolls in the pipe, it suppresses the roll rotation of the unit. The simplest way to solve this problem is to adopt an omnidirectional wheel that can travel holonomically. Since the omnidirectional wheel has a small wheel on the circumference, there is no constraint force in the direction perpendicular to the rotation direction of the wheel. Therefore, when the unit rolls in the pipe, the small wheel of the omnidirectional wheel rotates, and the frictional force can be suppressed.

B. Action of Normal Force That Promotes Roll Rotation

The principle of roll-rotation of the V-shaped unit in a curved pipe is considered, with a focus on the normal force. It is stated that when the front wheel of the unit enters the curved pipe, only one point contacts the wall. Fig. 2 shows that the cross-section of the curved pipe is egg-shaped, causing the normal force at this contact point to act in the normal direction of the egg-shaped curve. This normal direction (normal force) deviates from the y-axis of the relative coordinate system P as the unit enters the curved pipe, as shown in Fig. 3(a). In other words, this deviation is the moment arm that rotates the unit. To derive the length of this arm, the normal direction at an arbitrary point on the egg-shaped curve is first determined.

Differentiating equations (1) and (2) with respect to θ

$$\frac{dC_{a,X}(\theta)}{d\theta} = -\frac{D(R_c + \frac{D}{2}\cos\theta)\sin\theta}{2\sqrt{(R_c + \frac{D}{2}\cos\theta)^2 - a^2}} \tag{3}$$

$$\frac{dC_{a,Z}(\theta)}{d\theta} = -\frac{D}{2}\cos\theta. \tag{4}$$

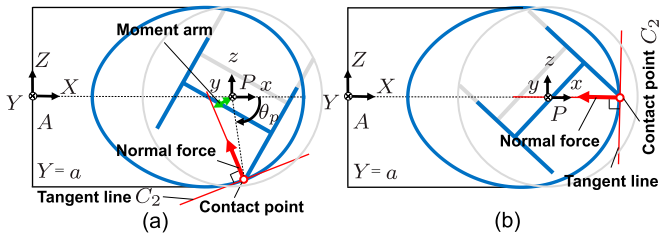

Fig. 3. Moment acting when traveling on a plane with $Y = a$. (a) represents the posture where the moment is acting, (b) represents the posture where the moment is not acting.

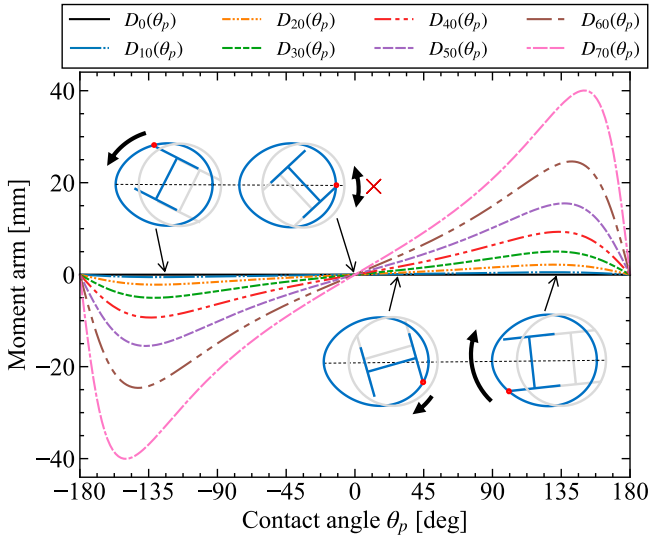

Fig. 4. Length of the moment arm when the contact point angle is θ_p.

The inclination $m_a(\theta_p)$ of the normal direction line at this time is obtained using equations (3) and (4) as follows:

$$m_a(\theta_p) = -\frac{dC_{a,X}(\theta_p)}{dC_{a,Z}(\theta_p)} = -\frac{(R_c + \frac{D}{2}\cos\theta_p)\tan\theta_p}{\sqrt{(R_c + \frac{D}{2}\cos\theta_p)^2 - a^2}}. \tag{5}$$

The normal direction line in z-x planes is obtained as follows using the slope:

$$z = m_a(\theta_p)(x - C_{a,X}(\theta_p)) + C_{a,Z}(\theta_p). \tag{6}$$

The distance from the rotation center $(R_c, a, 0)$ to the normal direction line (6), i.e., the length $D_a(\theta_p)$ of the moment arm that rotates the unit, is expressed as follows:

$$D_a(\theta_p) = \begin{cases} -d_a(\theta_p) & \text{if } -\frac{\pi}{2} \le \theta_p \le \frac{\pi}{2} \\ d_a(\theta_p) & \text{else} \end{cases} \tag{7}$$

$$d_a(\theta_p) = \frac{m_a(\theta_p)R_c - m_a(\theta_p)C_{a,X}(\theta_p) + C_{a,Z}(\theta_p)}{\sqrt{m_a^2(\theta_p) + 1}}. \tag{8}$$

The length $D_a(\theta_p)$ of the moment arm was calculated by moving a and changing θ_p, the results of which are given in Fig. 4.

The moment rotates the unit clockwise around the y-axis when the arm length is positive and counterclockwise when

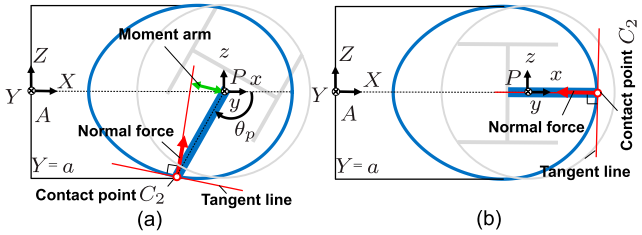

Fig. 5. Moment acting when traveling on a plane with Y = a by the V-shaped unit with a single wheel at each end. (a) and (b) in this figure correspond to the angles of entry in Fig. 3 (a) and (b).

the arm length is negative. At this moment, the rotation acts in the direction of converting the unit to a posture adapted to the curved pipe. The point to note is when the contact point angle θ_p is near 0°. In such a case, the moment arm is less likely to extend, even if the unit travels inside of the curved pipe. In other words, a large normal force is required for the rotation of the unit.

The V-shaped unit developed in a previous study [17] was able to travel passively through curved pipes at multiple entry angles. This was achieved by increasing the normal force through an active joint, making it easier to rotate due to the increased moment, even with a short moment arm. However, even with increased normal force, the unit cannot rotate when the moment arm is exactly zero (the contact point angle $\theta_p = 0$), as shown in Fig. 3(b).

C. Conditions for Traversing Curved Pipes in All Postures

The results of the static analysis so far can be summarized as follows.

1) There is no constraint force on the roll rotation around the pipe axis.
2) The curved pipe can be traversed even when the contact point angle θ_p of the front wheel is zero.

Based on the aforementioned conditions, a mechanism that can passively traverse curved pipes without the need for control is considered. First, an omnidirectional wheel is adopted for the wheel to reduce the frictional force of the rolling rotation around the pipe axis. Then, the mechanism should be able to traverse the curved pipe even when the contact point angle θ_p is zero. The simplest solution to this problem is to make the front and rear wheels of the V-shaped unit one wheel. The advantages of making it one wheel are as follows. Fig. 5(a) shows the moment arm when a unit with one wheel at each end enters in the same posture as Fig. 3(a), and Fig. 5(b) shows the posture when the length of the moment arm is zero (contact point angle $\theta_p = 0$).

1) In the same posture, the moment arm becomes longer than in the case of two wheels.
2) When the contact point angle $\theta_p = 0$, the unit can pass through it without rotating.

Therefore, the towed sensing unit is designed with a V-shape with one wheel at each end.

D. Preliminary Experiment

A preliminary experiment was conducted to pass through a curved pipe using a V-shaped unit with one wheel at each end,

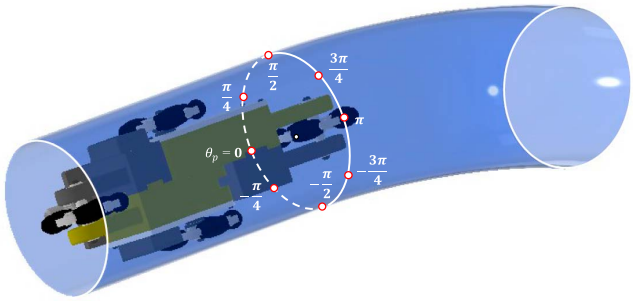

Fig. 6. Contact points of the front wheel when entering curved pipe.

which satisfies the conditions described in the previous section. As shown in Fig. 6, the contact points of the front wheel were shown when the entry angle was changed at intervals of $\pi/4$.

As shown in Fig. 7, trials were carried out at each entry angle of the curved pipe. As a result, it was confirmed that the unit could pass through the curved pipe at all entry angles. Therefore, even with a V-shaped shape linkage, the unit can pass through a curved pipe by making the front and rear wheels one wheel.

III. Pipeline Route Drawing System

A. Estimation of Current Coordinate Points From Earth Frame

Orientation estimation affects the accuracy of the pipeline route drawing, and thus, two methods are used and compared in this study. The first is the orientation estimation proposed by Madgwick et al. [15]. This method has lower computational cost and expected higher accuracy than the Kalman filter.

The second is the orientation estimation using the DMP function of the IMU (InvenSense, Inc., MPU-6050). This is a function that integrates the information of the gyroscopic sensor and the accelerometer. Since this function is calculated inside of the sensor, the computational cost can be greatly reduced more than the Madgwick filter [15].

The orientation obtained by the above two methods is converted to the travel direction $\hat{u}_{E,i}$ in the Earth frame E (XYZ) as in the previous method [13]. The coordinate point p_i at the ith sampling can be calculated in the following equation:

$$\boldsymbol{p_i} = \boldsymbol{p_{i-1}} + d_i \hat{\boldsymbol{u}}_{\boldsymbol{E,i}}. \tag{9}$$

Here, d_i is the traveling distance at the ith sampling measured from the encoder.

B. Identification of the Straight and Curved Pipes

From the previous method [13], it was found that the travel direction of the towed unit begins to face a different direction as the front wheel travels in the curved pipe, and when the center wheel enters the $j+1$th straight pipe, it travels in the straight line again. As shown in Fig. 8, the same tendency is observed even if the rotation direction of the curved pipe is not $\pi/2$. Therefore, the angle ψ_{D_i} between the travel direction $U_{E,j}$ at the jth straight pipe entry and the current direction of travel is calculated in (10). In order to estimate the transition point

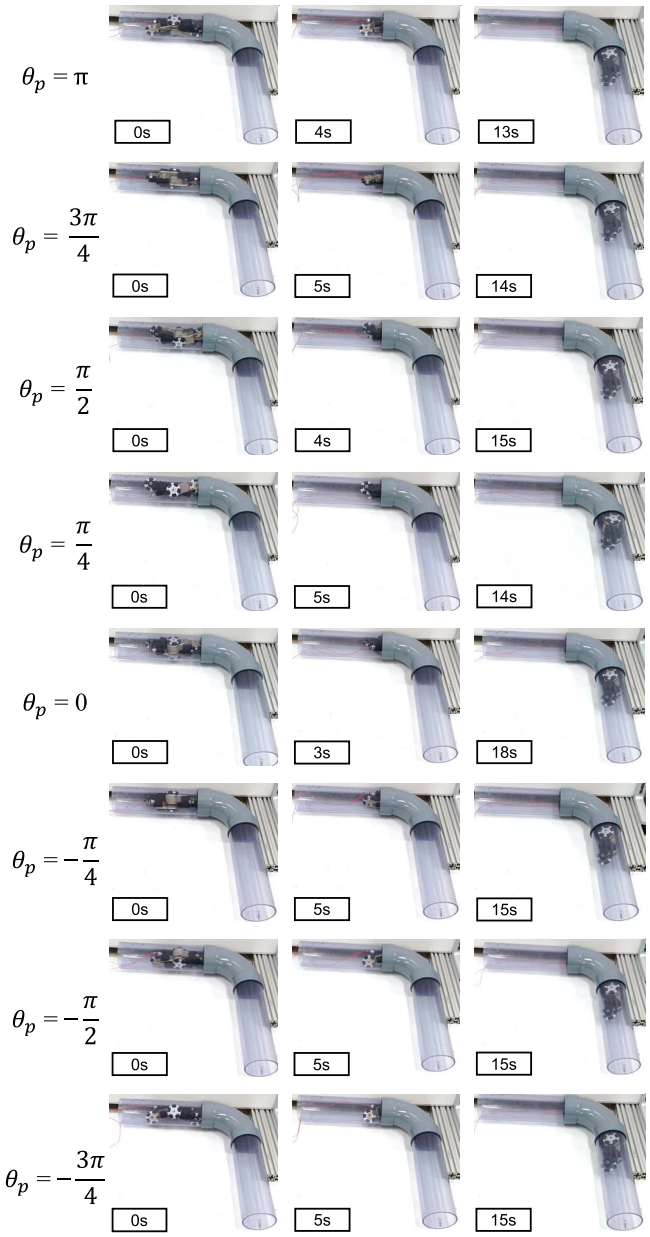

Fig. 7. Running experiment of the V-shaped unit at different entry angle of the curved pipe.

from the angle change of ψ_{D_i}, the response to the change is more important than the accuracy of the direction. Therefore, the estimation of the travel direction $u_{E,i}$ in this section is performed using only the gyroscopic sensor

$$\psi_{D_i} = \cos^{-1}\left(\boldsymbol{U}_{\boldsymbol{E},\boldsymbol{j}}^{\mathrm{T}}\boldsymbol{u}_{\boldsymbol{E},\boldsymbol{i}}\right). \tag{10}$$

Based on the above, the end point p_{e_j} of the jth straight pipe, i.e., the coordinate point when the front wheel of the towed unit enters the curved pipe, is determined as follows using ψ_{D_i} (see Fig. 8).

1) If the difference between the angle ψ_{D_i} and the angle 0.05 m prior $\psi_{D_i-0.05}$ exceeds $\pi/36$ rad (5°).

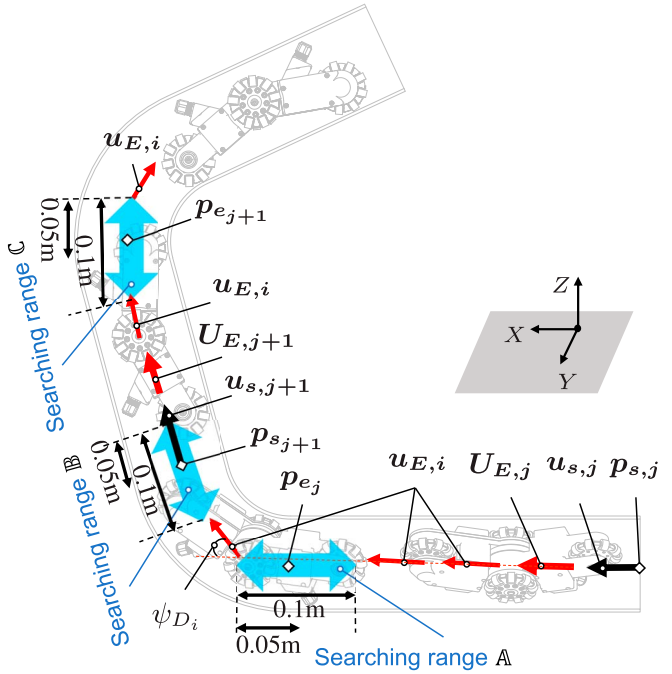

Fig. 8. Identification methods for the start and end points of curved pipes.

2) The end point is determined from the local minimum value of the angle change in the previous 0.1 m section (range $\mathbb{A}$).

The start point $p_{s_{j+1}}$ of the $j+1$th straight pipe, i.e., the coordinate point when the center wheels of the towed unit enters the $j+1$th straight pipe, is determined as follows using ψ_{D_i}.

1) If the difference between the angle ψ_{D_i} and the angle 0.05 m prior $\psi_{D_i-0.05}$ is less than $\pi/180$ rad (1°).
2) The start point is determined from the local maximum value of the angle change in the previous 0.1 m section (range $\mathbb{B}$).

The SciPy library of Python is used to detect the local minimum and maximum values. If the local minimum and maximum values do not exist in the range $\mathbb{A}$ and $\mathbb{B}$, respectively, the values at $\psi_{D_i-0.1}$ and ψ_{D_i} are applied to each transition point. Conversely, if multiple extrema are detected due to noise, after excluding the extrema with an angle change of $\pi/120$ rad or more, the local minimum closest to the current angle ψ_{D_i} is selected as the end point p_{e_j}, and the local maximum farthest from the current angle ψ_{D_i} is selected as the start point p_{s_j+1}. The start point p_{s_j} of the jth straight pipe and the end point $p_{e_{j+1}}$ of the $j+1$th straight pipe can also be estimated by applying the same method.

C. Estimation of Straight Pipe Direction After Passing Through Curved Pipes

The drawing of the $j+1$th straight pipe, i.e., the drawing from the coordinate point $p_{s_{j+1}}$ $(i = s_{j+1})$ to $p_{e_{j+1}}$ $(i = e_{j+1})$ is focused on (see Fig. 9). Since the straight pipe extends in a straight line, the first principal axis of the drawing from $p_{s_{j+1}}$ to $p_{e_{j+1}}$ roughly coincides with the $j+1$th straight pipe

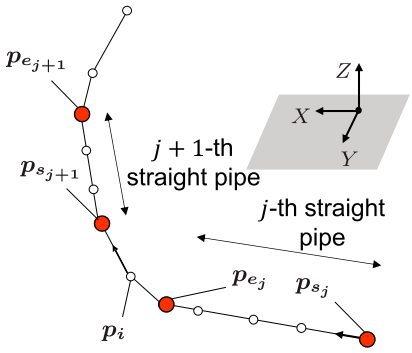

Fig. 9. Start and end points of the jth and $j+1$th straight pipes.

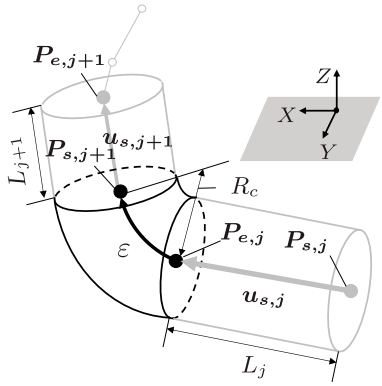

Fig. 10. Drawing method of the curved pipe.

axis. Therefore, the $j+1$th straight pipe direction $u_{s,j+1}$ is estimated using principal component analysis. The set of coordinate points during the $j+1$th straight pipe travel is $\boldsymbol{P}_{j+1}$.

The scale of each axis is different depending on the position of the initial coordinate $p_{s_{j+1}}$ of $\boldsymbol{P}_{j+1}$. Therefore, the data are centered in (11) and (12) to perform principal component analysis. The straight pipe direction $u_{s,j+1}$ obtained by principal component analysis is a straight line that minimizes the vertical distance from each point of $\bar{\boldsymbol{P}}_{j+1}$. $\bar{p}_{j+1}$ is the average of $p_{s_{j+1}}$ to $p_{e_{j+1}}$.

$$\bar{\boldsymbol{P}}_{j+1} = \begin{bmatrix} (\boldsymbol{p}_{\boldsymbol{s_{j+1}}} - \bar{\boldsymbol{p}}_{\boldsymbol{j+1}})^{\mathrm{T}} \\ \vdots \\ (\boldsymbol{p}_{\boldsymbol{e_{j+1}}} - \bar{\boldsymbol{p}}_{\boldsymbol{j+1}})^{\mathrm{T}} \end{bmatrix} \tag{11}$$

$$\bar{\boldsymbol{p}}_{\boldsymbol{j+1}} = \frac{1}{e_{j+1} - s_{j+1} + 1} \sum_{k=s_{j+1}}^{e_{j+1}} \boldsymbol{p}_{\boldsymbol{k}}. \tag{12}$$

The straight pipe direction $u_{s,j+1}$ is estimated from these 3-D points $\bar{\boldsymbol{P}}_{j+1}$. The covariance matrix $\boldsymbol{S}_{j+1}$ of $\bar{\boldsymbol{P}}_{j+1}$ is obtained in the following equation:

$$\boldsymbol{S}_{j+1} = \frac{1}{e_{j+1} - s_{j+1} + 1} \bar{\boldsymbol{P}}_{j+1}^{\mathrm{T}} \bar{\boldsymbol{P}}_{j+1}. \tag{13}$$

The eigenvalues λ and eigenvectors w of $\boldsymbol{S}_{j+1}$ are obtained by solving the eigenvalue problem in (14). The derivation uses the NumPy library of Python

$$\boldsymbol{S}_{j+1}\boldsymbol{w} = \lambda \boldsymbol{w}. \tag{14}$$

The first principal component is the eigenvector $\boldsymbol{w}_{\mathbf{max}}$ corresponding to the largest eigenvalue, and this axis becomes the axis of the $j+1$th straight pipe. The $j+1$th straight pipe direction $u_{s,j+1}$ is determined from the position of the first principal component score of the end point $p_{e_{j+1}}$ of the $j+1$th straight pipe in (15).

$$\boldsymbol{u}_{\boldsymbol{s,j+1}} : \begin{cases} -\boldsymbol{w}_{\mathbf{max}} & \text{if } (\boldsymbol{p}_{\boldsymbol{e_{j+1}}} - \bar{\boldsymbol{p}}_{\boldsymbol{j+1}})^{\mathrm{T}} \boldsymbol{w}_{\mathbf{max}} < 0 \\ \boldsymbol{w}_{\mathbf{max}} & \text{else} \end{cases} \tag{15}$$

D. Drawing of the Curved Pipes Between Two Straight Pipes

The trajectory of the curved pipe is uniquely determined if the start and end points of the curved pipe are known because $u_{s,j}$ and $u_{s,j+1}$ have already been estimated. In other words, if the end point $P_{e,j}$ and start point $P_{s,j+1}$ of the jth and $j+1$th straight pipes after the pipeline route is corrected are known, the curved pipe can be drawn as shown in Fig. 10. These points after the correction are estimated in (16)–(19). Here, the length of the jth straight pipe is L_j, the rotation angle of the curved pipe is ε, the radius of curvature is R_c, and the length of the link of the towed unit is L. Θ is the joint angle of the towed unit obtained from the geometric relationship between the straight pipe and the unit

$$\boldsymbol{P}_{\boldsymbol{e,j}} = \boldsymbol{P}_{\boldsymbol{s,j}} + L_j \boldsymbol{u}_{\boldsymbol{s_j}} \tag{16}$$

$$\boldsymbol{P}_{\boldsymbol{s,j+1}} = \boldsymbol{P}_{\boldsymbol{e,j}} + (\boldsymbol{u}_{\boldsymbol{s,j}} + \boldsymbol{u}_{\boldsymbol{s,j+1}}) R_c \tan\frac{\varepsilon}{2} \tag{17}$$

$$L_j = \sum_{i=s_j}^{e_j} d_i + L\sin\frac{\Theta}{2} \tag{18}$$

$$\varepsilon = \cos^{-1}(\boldsymbol{u}_{\boldsymbol{s,j}}^{\mathrm{T}} \boldsymbol{u}_{\boldsymbol{s,j+1}}). \tag{19}$$

IV. Rotational Direction Correction of the Curved Pipe Based on Its Classification

Many of the rotation directions of the curved pipes are present at $\pi/12$ intervals. Therefore, a correction method based on this rotation direction interval of the curved pipe is described.

A. Correction of the Straight Pipe Direction

Among the rotation angles at $\pi/12$ intervals, the angle φ closest to ε is selected. The angle φ can be obtained by using the floor function in the following equation:

$$\varphi = \frac{\pi}{12}\left\lfloor \frac{12}{\pi}\varepsilon + \frac{1}{2} \right\rfloor. \tag{20}$$

Fig. 11 shows the correction of the straight pipe direction using φ. The corrected straight pipe direction $U_{s,j+1}$ is calculated

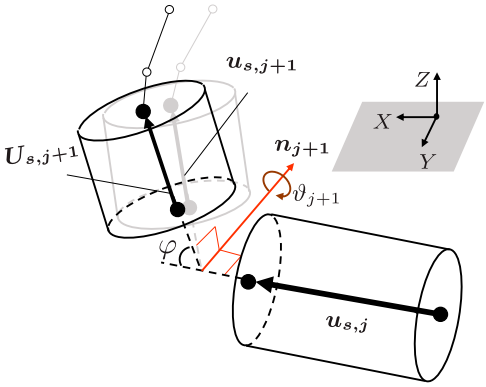

Fig. 11. Rotated $j+1$th straight pipe direction.

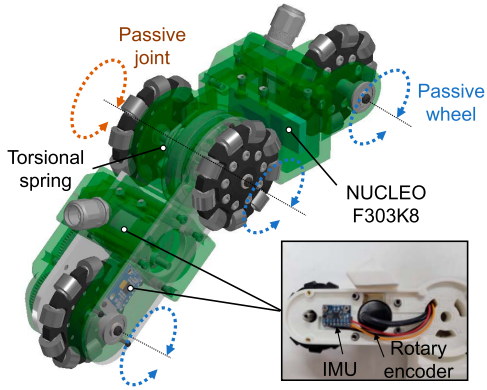

Fig. 12. Computer-aided design (CAD) model of the towed sensing unit (AIRo-mini-3.0).

by rotating $u_{s,j+1}$. The rotation axis n_{j+1} and rotation angle ϑ_{j+1} are obtained in the following equations:

$$\boldsymbol{n_{j+1}} = \frac{\boldsymbol{u_{s,j}} \times \boldsymbol{u_{s,j+1}}}{||\boldsymbol{u_{s,j}} \times \boldsymbol{u_{s,j+1}}||} \tag{21}$$

$$\vartheta_{j+1} = \varphi - \varepsilon. \tag{22}$$

From the Rodrigues rotation formula, the rotation matrix R_{j+1} that rotates ϑ_{j+1} around the rotation axis is obtained, and $U_{s,j+1}$ is obtained in the following equation:

$$\boldsymbol{U_{s,j+1}} = \boldsymbol{R_{j+1}}\, \boldsymbol{u_{s,j+1}}\,. \tag{23}$$

B. Correction of the Orientation of the Towed Unit

In the orientation correction by the accelerometer, the rotation around the gravity direction cannot be corrected. In addition, the correction by the magnetic sensor, which is widely used, is not suitable for pipelines [8]. Consequently, an orientation correction method based on the classification of the rotation direction of the curved pipe is proposed.

$u_{XY,s,j+1}$ and $U_{XY,s,j+1}$ are the vectors when $u_{s,j+1}$ and $U_{s,j+1}$ are projected onto the XY plane of the Earth frame E, and are obtained in the following equation:

$$u_{XY,s,j+1} = \boldsymbol{u_{s,j+1}} - \left(\boldsymbol{u}_{s,j+1}^{\mathrm{T}} \boldsymbol{u_Z}\right) \boldsymbol{u_Z} \tag{24}$$

$$U_{XY,s,j+1} = \boldsymbol{U_{s,j+1}} - \left(\boldsymbol{U}_{s,j+1}^{\mathrm{T}} \boldsymbol{u_Z}\right) \boldsymbol{u_Z}. \tag{25}$$

Here, $\boldsymbol{u_z} = \begin{bmatrix} 0 & 0 & 1 \end{bmatrix}^{\mathrm{T}}$.

The angle α_{j+1} between $u_{XY,s,j+1}$ and $U_{XY,s,j+1}$ is obtained in the following equation:

$$\alpha_{j+1} = \cos^{-1} \frac{\boldsymbol{u}_{\boldsymbol{XY,s,j+1}}^{\mathrm{T}} \boldsymbol{U_{XY,s,j+1}}}{||\boldsymbol{u_{XY,s,j+1}}||\ ||\boldsymbol{U_{XY,s,j+1}}||}. \tag{26}$$

The angle α_{j+1} calculated here is the deviation of the rotation around the gravity direction. The rotation axis γ_{j+1} that performs this rotation is obtained in the following equation:

$$\gamma_{j+1} = \frac{\boldsymbol{u_{XY,s,j+1}} \times \boldsymbol{U_{XY,s,j+1}}}{||\boldsymbol{u_{XY,s,j+1}} \times \boldsymbol{U_{XY,s,j+1}}||}. \tag{27}$$

The corrected quaternion ${}^{S}_{E}\hat{\mathrm{Q}}_{\mathrm{est},s_i}$ is obtained using the rotation angle α_{j+1} and rotation axis γ_{j+1} in the following equation:

$${}^{\boldsymbol{S}}_{\boldsymbol{E}}\hat{\mathrm{Q}}_{\boldsymbol{\mathrm{est},i}} = \begin{bmatrix} \cos\left(\dfrac{\alpha_{j+1}}{2}\right) \\ \boldsymbol{\gamma_{j+1}} \sin\left(\dfrac{\alpha_{j+1}}{2}\right) \end{bmatrix}^{\mathrm{T}} \otimes {}^{\boldsymbol{S}}_{\boldsymbol{E}}\hat{\boldsymbol{q}}_{\boldsymbol{\mathrm{est},i}}. \tag{28}$$

However, if the orientation is calculated on the microcomputer side of the towed unit, the rotation is the cumulative sum from α_1 to α_{j+1}.

V. Experiment

A. The Developed Sensing System and Experimental Environment

The towed sensing unit (AIRo-mini-3.0) is pulled by the self-propelled in-pipe inspection robot (AIRo-2.6), as shown in Fig. 1. The robot (AIRo-2.6) consists of three passive joints using torsion springs and runs while stretching the pipe. In addition, the joint part was changed to metal from the previous robot [13] to improve the strength. The robot uses a hemispherical wheel inspired by Tadakuma et al. [18] at both ends, and the robot can be rolled by rotating this wheel. The drive wheel and the roll wheel of the robot are connected to the printed circuit board, respectively. The operator controls the robot via CAN–BUS communication from the game pad, but automatic running of the robot with the same shape has already been realized in our previous study [19].

Fig. 12 shows the internal structure of The towed sensing unit (AIRo-mini-3.0). The unit (AIRo-mini-3.0) also runs while stretching the pipe with one passive joint using a torsion spring. However, no actuator is installed. A rotary encoder (OMRON Corporation., E6A2-CW3C 500P/R, less than \$90) is attached to the front passive wheel, and an IMU (InvenSense Inc., MPU-6050, less than \$3) is attached to the front link. A microcontroller (STMicro, Nucleo F303K8) is installed on the rear of the unit, and the information of the IMU and the encoder is sent to the computer via USB serial.

The wheels of the robot and the towed unit are all omnidirectional wheels. These are made of nitrile butadiene rubber (NBR)

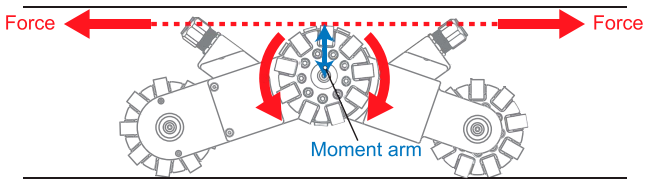

Fig. 13. Rotation on the joint caused by pulling power applied to the cable.

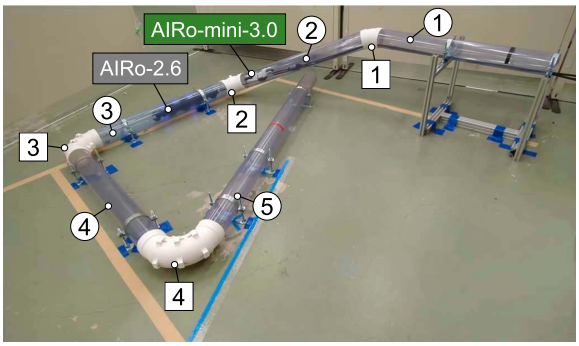

Fig. 14. Pipeline course when straight pipes are not along the coordinate axes

used in previous research [20], which can achieve durability and high friction.

As shown in Fig. 13, the link of the towed unit (AIRo-mini-3.0) is designed to close due to the cable tension. Therefore, the more the cable tension increases, the less likely the measurement wheel is to slip.

The pipeline course used in the experiment is presented in Fig. 14. The rotation angles of the curved pipes are $\pi/6$, $\pi/3$, $\pi/2$, and $2\pi/3$. The straight pipes ①, ③, ④, and ⑤ are installed horizontally using a level, and the installation angle and height of each pipe are measured using a protractor and a tape measure. The inner diameter (4-in) and radius of curvature (128 mm) of the pipe are known information.

B. Experimental Results

In this experiment, drawing is performed using two types of orientation estimation methods: Madgwick filter and DMP. Fig. 15 presents a comparison between the drawn route and the actual pipeline model using the two methods. In this drawing, the rotation direction of the curved pipe is corrected using the proposed method in Section IV.

As shown in Fig. 15, it can reproduce the shape of the actual pipeline course. First, the estimated length of each straight pipe and the actual pipeline length are shown in Table II.

As indicated in Table II, the mean absolute error (MAE) of the estimated length of the five straight pipes was 1.38%. The error range is also ±2.6%, and thus the length of the straight pipe can be estimated with high accuracy. This is because, as described in A of this section, the measurement wheels of the towed unit were designed to prevent them from moving away from the pipe wall.

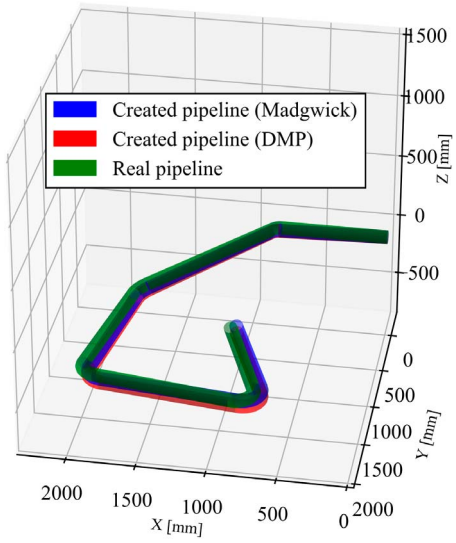

Fig. 15. Difference between the drawn route and the true pipeline route when the curved pipe's rotation direction is corrected.

TABLE II
MEASURED LENGTH OF EACH STRAIGHT PIPE AND THEIR ERRORS

Pipe	True Value (m)	Measured Value (m)	Error (%)
①	0.792	0.808	2.0
②	1.020	0.987	−3.2
③	1.015	1.016	0.1
④	1.015	1.024	0.9
⑤	0.847	0.841	−0.7
Mean absolute error (MAE)			1.38
Error range			±2.6

Second, the accuracy of the straight pipe direction estimation is evaluated. The evaluation method is the angle between the actual direction of each straight pipe and the estimated direction of each pipe. The error angle is given in Table III.

As shown in Table III, the error of the Madgwick filter is smaller in the first half of the pipeline, but the error of DMP is smaller in the second half. This is believed to be a consequence of the accuracy of the orientation correction. The main orientation changes of the towed unit running in the pipes are roll rotation in the pipes and inclination of the orientation due to the inclination of the pipes.

Considering the measurement of the first half of the pipeline, when inserting the unit into the first pipe, all the wheels are arranged to be horizontal to the pipe axis. Therefore, in the first half of the pipeline course, roll rotation is less likely to occur, and in the straight pipe ②, the influence of the inclination of the pipeline is greater than that of the roll rotation. Then, since the curved pipes 3 and 4 are rotating in the horizontal plane, it is considered that the influence of the roll rotation becomes larger than that of the inclination of the pipeline in the latter half. In other words, the correction accuracy of the inclination of the orientation is considered to be better for the Madgwick filter, and the correction accuracy of the roll rotation is considered to be better for DMP.

TABLE III
MEASURED DIRECTION VECTOR OF EACH PIPE AND THEIR ERRORS WHEN THE CURVED PIPE'S ROTATION DIRECTION IS CORRECTED

Pipe	True vector	Measured vector		Error angle [°]	
		Madgwick	DMP	Madgwick	DMP
①	$\begin{bmatrix}1.000\\0.000\\0.000\end{bmatrix}$	$\begin{bmatrix}1.000\\-0.001\\-0.029\end{bmatrix}$	$\begin{bmatrix}0.999\\-0.002\\-0.036\end{bmatrix}$	1.66	2.09
②	$\begin{bmatrix}0.866\\0.365\\-0.341\end{bmatrix}$	$\begin{bmatrix}0.856\\0.379\\-0.351\end{bmatrix}$	$\begin{bmatrix}0.854\\0.372\\-0.364\end{bmatrix}$	1.08	1.53
③	$\begin{bmatrix}0.161\\0.987\\0.000\end{bmatrix}$	$\begin{bmatrix}0.144\\0.990\\-0.005\end{bmatrix}$	$\begin{bmatrix}0.148\\0.989\\-0.017\end{bmatrix}$	1.02	1.25
④	$\begin{bmatrix}-0.987\\0.161\\0.000\end{bmatrix}$	$\begin{bmatrix}-0.989\\0.144\\0.023\end{bmatrix}$	$\begin{bmatrix}-0.989\\0.148\\0.012\end{bmatrix}$	1.62	1.00
⑤	$\begin{bmatrix}0.354\\-0.935\\0.000\end{bmatrix}$	$\begin{bmatrix}0.370\\-0.929\\0.016\end{bmatrix}$	$\begin{bmatrix}0.366\\-0.930\\0.008\end{bmatrix}$	1.39	0.89
Mean error				1.35	1.35

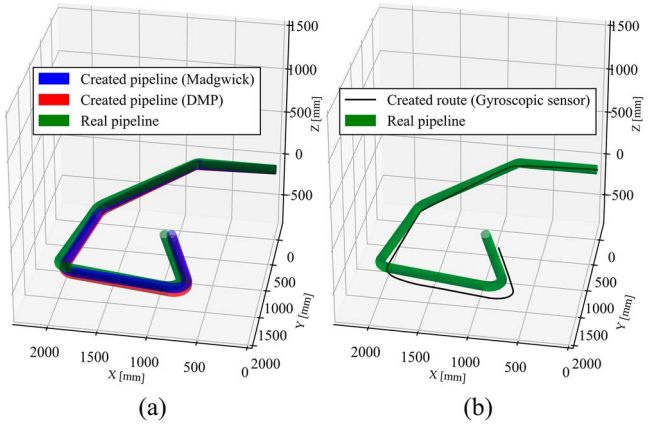

Fig. 16. (a) Difference between the drawn route and the true pipeline route when the curved pipe's rotation direction is not corrected. (b) Difference between the drawn route without proposed methods and the true pipeline route.

TABLE IV
FINAL POINTS OF THE DRAWN ROUTE AND ERRORS

True point [m]	Measured point [m]		Error distance [m]	
	Madgwick	DMP	Madgwick	DMP
$\begin{bmatrix}1.031\\0.833\\-0.385\end{bmatrix}$	$\begin{bmatrix}0.990\\0.830\\-0.366\end{bmatrix}$	$\begin{bmatrix}0.988\\0.824\\-0.426\end{bmatrix}$	0.045	0.060

TABLE V
FINAL POINTS WITHOUT THE ROUTE CORRECTION

True point [m]	Measured point [m]	Error distance [m]
	Gyroscopic sensor	Gyroscopic sensor
$\begin{bmatrix}1.031\\0.833\\-0.385\end{bmatrix}$	$\begin{bmatrix}0.893\\0.776\\-0.583\end{bmatrix}$	0.248

Based on the above, it is considered that the Madgwick filter is better in an environment in which a large number of pipeline inclinations are assumed, and DMP is better in a flat environment or a long-distance course where the influence of roll rotation is increased. However, even in the straight pipe ④, where the difference was the largest, the difference was small at 0.62°. In addition, the measurement errors of the final points are small, 0.045 m for the Madgwick filter and 0.060 m for DMP, as shown in Table IV. In other words, both methods can measure with high accuracy.

The drawing result when the classification of the rotation direction of the curved pipe was unknown is shown in Fig. 16(a). The difference between the measured route and the actual pipeline course is large, but the shape of the pipeline can be reproduced. In other words, it is considered that it can be sufficiently utilized for inspection and maintenance management for pipeline facilities with many unknown elements.

Finally, the route drawn without using the proposed method is presented in Fig. 16(b). In this case, the orientation is estimated only by the gyroscopic sensor. As shown in Fig. 16(b), the drawn route is far from the actual pipeline course. Furthermore, the measured error of the final point is 0.248 m (Table V), which is approximately four times larger than that in Table IV, and thus the validity of the proposed method is demonstrated.

VI. DISCUSSION

The remaining issues with the drawing method proposed in this study are summarized as follows. The first is that it is assumed that the inner diameter and the curvature radius of the pipeline are known. There are many pipeline courses where the inner diameter is constant, and the curvature radius of the curved pipe is also often one type for simplifying construction. However, in actual environments, there are also pipelines called increasers where the inner diameter changes in the middle, and there are also pipeline environments where the curvature radius is unknown because they are buried underground. To solve this problem, it is sufficient to add a sensor that measures the joint angle of the towed unit. Since there is only one joint and the sensor size is small, it does not affect miniaturization of the system. If the joint angle change is known, the inner diameter change of the pipeline can be detected, and furthermore, the deformation of the pipeline can be measured. In addition, since the shape change of the towed unit in the curved pipe can be measured, it can be used to estimate the curvature radius. The search range (0.05 or 0.1 m) which was mentioned in the Section IV could be also adjusted by estimating the pipe diameter and the radius of the curvature.

The second is the estimation of the slip of the measurement wheels. As mentioned previously, the measurement wheels of the developed unit are designed to be less likely to move away from the pipe wall by utilizing the cable tension. Therefore, the slip of the wheels is taken into account from the hardware perspective, but the risk exists that they may slip due to the viscous debris in the pipeline. If this slip occurs, it will become difficult to calculate the actual running distance from the rotation speed of the measurement wheels. Regarding this issue, it could be solved by using the accelerometer already installed in the unit.

If the slip can be estimated from the software point of view, the accuracy of the route drawing can be further improved.

The third is that the proposed method does not assume a pipeline course with T-branches. There are many studies that assume T-branches [2], [7], [8], [10], [21], but all of them target large pipe diameters. The method proposed in this study assumes that the pipeline course is composed only of curved pipes. Although T-branches are not as common as curved pipes, the practicality will increase if they can be handled. In general, the challenge for a robot to traverse a T-branch pipe is how to actively direct the robot body to the next pathway. However, in the case of a towed unit, the robot is pulled and runs, so using the cable tension at that moment allows for passive selection of the travel path. In addition, even when running from a straight pipe to a T-branch pipe, the direction of travel changes in the same way, so it is considered that the method proposed in this study can be applied. In the future, we will consider a method that prevents the towed unit from getting stuck at the corner of the T-branch pipe regardless of the posture of the unit after the robot passes through the T-branch pipe.

VII. Conclusion

In this study, a pipeline route drawing system that combines a towed sensing unit without actuators and a self-propelled in-pipe inspection robot was proposed. Many existing methods use external sensors, but in this method, the type of pipeline was classified only from low cost internal sensors, and the shape of the pipeline was reproduced using that information. Therefore, it was not affected by the illumination in the pipeline. Since this system does not depend on the shape of the leading robot, it can be applied to robots that have no room to install new sensors due to spatial constraints in the pipeline just by connecting the unit to the rear. In addition, since only one pair of an IMU and an encoder were used as sensors, it can be downsized, and of course, it can be applied to large robots. In the future, research aimed at drawing pipeline routes in actual environments will be conducted.

References

[1] P. Hansen, H. Alismail, B. Browning, and P. Rander, "Stereo visual odometry for pipe mapping," in *Proc. IEEE/RSJ Int. Conf. Intell. Robots Syst.*, 2011, pp. 4020–4025.

[2] P. Hansen, H. Alismail, P. Rander, and B. Browning, "Pipe mapping with monocular fisheye imagery," in *Proc. IEEE/RSJ Int. Conf. Intell. Robots Syst.*, 2013, pp. 5180–5185.

[3] A. N. Chand, N. Zuhdi, A. Mansor, A. Iqbal, F. Rustam, and W. Baur, "An industrial robot for firewater piping inspection and mapping," in *Proc. IEEE/RSJ Int. Conf. Intell. Robots Syst.*, 2021, pp. 2314–2321.

[4] H. Zhang et al., "LNC assisted localization and mapping in pipe environment," in *Proc. IEEE/RSJ Int. Conf. Intell. Robots Syst.*, 2022, pp. 5180–5185.

[5] H. Lim, J. Y. Choi, Y. S. Kwon, E. J. Jung, and B. J. Yi, "SLAM in indoor pipelines with 15mm diameter," in *Proc. IEEE Int. Conf. Robot. Automat.*, 2008, pp. 4005–4011.

[6] Y. Kwon and B. Yi, "Design and motion planning of a two-module collaborative indoor pipeline inspection robot," *IEEE Trans. Robot.*, vol. 28, no. 3, pp. 681–696, Jun. 2012.

[7] J. S. Lee, S. G. Roh, D. W. Kim, H. Moon, and H. R. Choi, "In-pipe robot navigation based on the landmark recognition system using shadow images," in *Proc. IEEE Int. Conf. Robot. Automat.*, 2009, pp. 1857–1862.

[8] D. H. Lee, H. Moon, J. C. Koo, and H. R. Choi, "Map building method for urban gas pipelines based on landmark detection," *Int. J. Control Automat. Syst.*, vol. 11, no. 1, pp. 127–135, 2013.

[9] A. Ahrary, Y. Kawamura, and M. Ishikawa, "A laser scanner for landmark detection with the sewer inspection robot KANTARO," in *Proc. IEEE/SMC Int. Conf. Syst. Syst. Eng.*, 2006, pp. 310–315.

[10] D. H. Lee, H. Moon, and H. R. Choi, "Landmark detection methods for in-pipe robot traveling in urban gas pipelines," *Robotica*, vol. 34, pp. 601–618, Mar. 2016.

[11] H. Jang, T. Y. Kim, Y. C. Lee, Y. H. Song, and H. R. Choi, "Autonomous navigation of in-pipe inspection robot using contact sensor modules," *IEEE/ASME Trans. Mechatron.*, vol. 27, no. 6, pp. 4665–4674, Dec. 2022.

[12] D. Guo, Z. Yuan, S. Bao, J. Yuan, S. Ma, and, L. Du, "Visualized small-size pipeline model building using multilink-articulated wheeled in-pipe inspection robot," in *Proc. IEEE Int. Conf. Real-Time Comput. Robot.*, 2021, pp. 492–497.

[13] A. Kakogawa, C. Hirose, and S. Ma, "A standards-based pipeline route drawing system using a towed sensing unit," in *Proc. IEEE/RSJ Int. Conf. Intell. Robots Syst.*, 2022, pp. 7167–7173.

[14] A. Kakogawa and S. Ma, "Design of a multilink-articulated wheeled pipeline inspection robot using only passive elastic joints," *Adv. Robot.*, vol. 32, no. 1, pp. 37–50, 2018.

[15] S. O. H. Madgwick, A. J. L. Harrison, and R. Vaidyanathan, "Estimation of IMU and MARG orientation using a gradient descent algorithm," in *Proc. IEEE Int. Conf. Rehabil. Robot.*, 2011, pp. 1–7.

[16] Y. Oka, A. Kakogawa, and S. Ma, "Control technique of a V-shaped in-pipe robot composed of two underactuated roll-pitch joints," *J. Robot. Mechatron.*, vol. 36, no. 4, pp. 205–216, 2022.

[17] A. Kakogawa and S. Ma, "An in-pipe inspection module with an omnidirectional bent-pipe self-adaptation mechanism using a joint torque control," in *Proc. IEEE/RSJ Int. Conf. Intell. Robots Syst.*, 2019, pp. 4347–4352.

[18] K. Tadakuma, "Tetrahedral mobile robot with novel ball shape wheel," in *Proc. 1st IEEE/RAS-EMBS Int. Conf. Biomed. Robot. Biomechatron.*, 2006, pp. 946–952.

[19] A. Kakogawa, Y. Komurasaki, and S. Ma, "Shadow-based operation assistant for a pipeline-inspection robot using a variance value of the image histogram," *J. Robot. Mechatron.*, vol. 31, no. 6, pp. 772–780, 2019.

[20] A. Kakogawa, K. Murata, and S. Ma, "Automatic T-branch travel of an articulated wheeled in-pipe inspection robot using joint angle response to environmental changes," *IEEE Trans. Ind. Electron.*, vol. 70, no. 7, pp. 7041–7050, Jul. 2023.

[21] S. Kazeminasab and M. K. Banks, "A localization and navigation method for an in-pipe robot in water distribution system through wireless control towards long-distance inspection," *IEEE Access*, vol. 9, pp. 117496–117511, 2021.

Chihiro Hirose received the master's degree in mechanical engineering from Ritsumeikan University, Shiga, Japan, in 2024.

He is currently working as an Engineer with Toyota Motor Corporation, Toyota, Japan. His research interest includes development of the sensing system for in-pipe inspection robots.

Shunsuke Ota received the master's degree in mechanical engineering from Ritsumeikan University, Shiga, Japan, in 2022.

He is currently working as an Engineer with Panasonic Industry Company, Ltd., Tokyo, Japan. His research interest includes development of the friction reduction mechanism for in-pipe inspection robots.

Atsushi Kakogawa (Member, IEEE) received the Ph.D. degree in mechanical engineering from Ritsumeikan University, Shiga, Japan, in 2015.

He joined the Department of Robotics, Ritsumeikan University, as an Assistant Professor, in 2015; as a Lecturer, in 2019; where he is currently working as an Associate Professor. He was a Visiting Assistant Professor with the University of Waterloo, Waterloo, ON, Canada, in 2017. His research interests include the design and control of robots using viscoelasticity and differential mechanisms and robotic in-pipe inspection as an example of snake-like robot applications.

Shugen Ma (Fellow, IEEE) received the Dr.Eng. degree in mechanical engineering science from the Tokyo Institute of Technology, Tokyo, Japan, in 1991.

From 1991 to 1992, he was a Researcher with Komatsu Ltd., Tokyo, Japan. From 1992 to 1993, he was a Visiting Scholar with the University of California, Riverside, CA, USA. In July 1993, he joined as an Assistant Professor with the Department of Systems Engineering, Ibaraki University, Hitachi, Japan. In October 2005, he joined as a Professor with the Department of Robotics, Ritsumeikan University, Shiga, Japan. In December 2023, he joined the Hong Kong University of Science and Technology (Guangzhou), Guangzhou, China, where he is currently a Professor. He is also the Director of the Shanghai Robotics Institute, Shanghai University, Shanghai, China. His research interests include the design and control theory of new types of robots, field robotics, and biorobotics.

Dr. Ma is a fellow of the Japan Society of Mechanical Engineers and a member of the Society of Instrument and Control Engineers of Japan and the Robotics Society of Japan. He is the General Chair of the 2022 IEEE/RSJ International Conference on Intelligent Robots and Systems. He was an Associate Editor for IEEE TRANSACTIONS ON ROBOTICS from 2003 to 2007 and an Editor for *Advanced Robotics* in 2007. He serves many societies and conferences.